

¹ Coexistence of Turbulence and Discrete Modes in the ² Solar Wind

S. Ghosh,¹ D. J. Thomson,² W. H. Matthaeus,³ and L. J. Lanzerotti⁴

S. Ghosh, Space Department, Johns Hopkins University - Applied Physics Laboratory, Laurel, MD 20723, USA. (ron.ghosh@jhuapl.edu)

D. J. Thomson, Department of Mathematics and Statistics, Queens University, Kingston, Ontario, Canada. K7L 3N6 (djt@mast.queensu.ca)

W. H. Matthaeus, Bartol Research Institute, University of Delaware, Newark, DE 19716, USA. (whm@udel.edu)

L. J. Lanzerotti, New Jersey Institute of Technology, University Heights, Newark NJ 07102, USA. (ljl@njit.edu)

¹Space Department, Johns Hopkins

3 **Abstract.** Motivated by apparently contradictory reports of turbulence
4 and discrete frequency wave-like signals in the interplanetary medium, we
5 employ numerical simulations to investigate the persistence of wave-like spa-
6 tial structures in the presence of strong low-frequency turbulence. We seek
7 to identify the time scales and other conditions that permit them to remain
8 as identifiable structures in the turbulent medium. The wave-like structures
9 are initialized as discrete modes in wavenumber in a series of spectral method
10 magnetohydrodynamic turbulence computations. We find that discrete modes
11 can survive from one to many nonlinear times, and that the main factor that
12 determines their survivability is the separation from turbulence in parallel

University - Applied Physics Laboratory,

Laurel, Maryland, USA.

²Queens University, Kingston, Ontario,

CANADA.

³Bartol Research Institute and

Department of Physics and Astronomy,

University of Delaware, Newark, Delaware,

USA.

⁴New Jersey Institute of Technology,

Newark, New Jersey, USA.

¹³ wavenumber. This corresponds to a separation in their corresponding Alfvén
¹⁴ mode frequency.

1. Introduction

15 Observations show that numerous frequencies obtained by spectrum analysis of time
16 series of interplanetary magnetic fields and particle densities agree closely with those
17 predicted for solar gravity, g , and pressure, p , mode oscillations (see *Thomson et al.*
18 [1995], hereinafter TML). These observations are made at 1 AU by the ACE spacecraft
19 and seen beyond 1 AU in Ulysses and Voyager II data, (TML and *Thomson et al.* [2001]).
20 It transpires that questions immediately arise [*Roberts et al.*, 1996] as to how the point
21 spectral features of these modes, which we call discrete modes, can persist not only through
22 the corona, but through the additional dynamical processing expected in the solar wind
23 during its transit from the source regions to the point of observation.

24 Here we examine the specific question of whether a wave-like spatial structure embedded
25 initially in a field of turbulent fluctuations can be maintained during subsequent turbulent
26 dynamical evolution. Using numerical simulation, we identify conditions in which the
27 wave-like discrete mode can be destroyed within a nonlinear-interaction time scale, and
28 other conditions in which it can be maintained for many nonlinear-interaction times. This
29 has implications for models of observed solar wind fluctuations that have what appears
30 to be a mode structure.

31 In the next section we briefly review the observational and the theoretical backgrounds.
32 Section 3, describes the numerical simulation method, the strategy of the numerical com-
33 putations, and the particular initial conditions and driving that we employ. In Section 4
34 we provide a description of the numerical results. In Section 5 we discuss the implications

35 for solar wind observations and for models of generation of interplanetary and coronal
36 fluctuations.

2. Background and Observations

37 Solar wind fluctuations are usually regarded as a more or less featureless random su-
38 perposition of fluctuations. These may have an origin as coronal waves and turbulence,
39 or as *in situ* generated turbulence or as some mixture of these *Tu and Marsch [1995]*.
40 Regardless of the origin, the prevalent view is that the baseline description is a spectrum
41 that is of the broad band rather than of the point spectral type.

42 However there are intriguing observations that are at odds with this view. For example,
43 the power spectrum of time series of charged particle fluxes from the HISCALE detector
44 on the Ulysses spacecraft [*Lanzerotti et al., 1992*] often contain periodic components that
45 are not simply harmonics of solar rotation. TML noted that the observed frequencies,
46 associated with periods ranging from about an hour to a few minutes, were consistent with
47 the frequency range of solar *p*-modes, and solar gravity, or *g*-modes. Similar frequencies
48 were subsequently reported at 1 AU in ACE data and beyond 1 AU in Ulysses data
49 [*Thomson et al., 2001*]. Moreover, in *Thomson et al. [2007]* it was shown that the modes
50 are both coherent and their ellipticities are preserved between ACE and Ulysses.

51 To make the issues clear we present an example of this type of analysis here. An estimate
52 of the power spectrum of solar wind proton density data between 200 and 500 μHz is
53 shown in Figure 1. The data is from the SWEPAM instrument on ACE, *McComas et al.*
54 [*1998*], between Feb. 5, 1998 and Nov. 23, 2005, a span of 1899 days. The spectrum
55 was estimated using multitaper methods, *Thomson [1982]*; *Thomson et al. [2007]* with
56 the base level estimated as in *Thomson et al. [2001]*. Because the frequency resolution

57 in this estimate is 3.97 nHz plotting this spectrum directly gives an uninformative smear
 58 and, consequently, we have plotted quantiles. These are initially taken over $\pm 0.4 \mu\text{Hz}$
 59 intervals offset 50%, then smoothed over $\pm 2 \mu\text{Hz}$. Over this range the overall shape has
 60 the $f^{-5/3}$ dependence expected from Kolmogorov turbulence. However, the ratio of the
 61 90% to the 5% curve is ~ 5.8 , considerably larger than the factor of 2.46 expected for a χ_{22}^2
 62 distribution. The discussion in *Thomson et al.* [2001] shows that a probable explanation
 63 of this discrepancy is that the distribution is not a *central* χ_{22}^2 , but a mixture of central
 64 and non-central distributions, non-central at modal frequencies and central between.

65 The insert in this plot shows the spectrum between 400 and 410 μHz . The probability
 66 that fluctuations in the estimated spectrum (assumed to be generated by Gaussian noise
 67 with a $f^{-5/3}$ spectrum for frequencies above $\sim 136 \mu\text{Hz}$) will be below the horizontal lines
 68 is indicated. The high peak in the insert is at a synodic frequency of $\approx 404.157 \mu\text{Hz}$
 69 and is so far above background that the probability of such an excursion from a smooth
 70 spectrum is $\lesssim 6 \times 10^{-16}$. Measured at a spectral level of 3.2×10^7 the width of this peak
 71 is $\approx 39 \text{ nHz}$ very close to the nominal bandwidth, 42.7 nHz, of the estimate. It has close,
 72 symmetric sidebands at ~ 403.818 and $404.529 \mu\text{Hz}$, *i.e.* offset by ~ -339 and $+372 \text{ nHz}$,
 73 respectively. There is some evidence of fine splitting, asymmetry, and possibly frequency
 74 modulation in all three peaks, so the frequencies may be accurate to about $\pm 20 \text{ nHz}$. Both
 75 sidebands have probabilities of $\lesssim 5 \times 10^{-6}$. This mode is close to the predicted frequency
 76 of the solar $p_{0,2}$ mode, $\sim 404.45 \mu\text{Hz}$ [*Provost et al.*, 2000] and is essentially identical to
 77 that of the peak shown at $\sim 404.05 \pm 1.1 \mu\text{Hz}$ in Fig. 11 of *Thomson et al.* [2007]. By
 78 standard theory, $p_{0,2}$ should not be split, so this splitting may reflect structure in the Sun.
 79 Further discussion of these fascinating details is beyond the scope of this paper, but the

80 important thing to remember is that, even allowing for the $\sim 250,000$ samples used to
81 compute these spectra, such low probabilities cannot be explained except by admitting
82 that discrete modes coexist with turbulence in the solar wind.

83 There are a number of additional reports in the literature that identify discrete modes
84 that persist in solar wind fluctuations for long times or long distances. Our primary
85 purpose here is not to support or controvert those claims but rather to examine the basic
86 physical issues that would influence the possibility of survival of a wave like structure in
87 strong evolving turbulence.

88 In particular there have been several objections to the TML discrete mode-picture based
89 on criticism of statistical analysis (e.g., *Hoogeveen and Riley* [1998]; *Denison and Walden*
90 [1999]) and answered in *Thomson et al.* [2001]. Perhaps the mostly clearly stated physical
91 objection is that of *Roberts et al.* [1996], who argue that turbulence will not permit such
92 wave modes to persist long enough to be detected. The essence of that objection is that
93 a cascade of the Kolmogoroff type necessarily processes fluctuations at all scales, so that
94 any coherence is lost in a time scale of the order of an eddy turnover time. This time
95 scale being of the same order as that required to generate an inertial range, along with
96 the observation of an inertial range powerlaw spectrum, combines to imply that any such
97 wave signature should be lost by 1 AU. *Roberts et al.* [1996] provide a one-dimensional
98 (1D) simulation to support their assertion that turbulence cannot support the persistence
99 of coherent wave modes. It is this issue that we re-address here.

100 In recent years understanding of three dimensional (3D) MHD turbulence has improved,
101 and one can productively revisit this basic physics question in several ways. Turbulence
102 typically does not generate discrete frequency modes, but does it permit them to persist

103 if they are supplied at a boundary or by initial data? This can be posed as a basic physics
104 question in turbulence theory: *To what extent can a wave-like feature in the time domain*
105 *persist in space in the presence of turbulence?*

106 One way of looking at this question was devised by *Dmitruk et al.* [2004]. In this case
107 numerical simulations were set up using a simple three-dimensional coronal model that
108 is ordinarily used to investigate heating driven by turbulence. The model has a uniform
109 mean magnetic field (in the vertical z-direction) and is driven by stirring motions in the
110 transverse x-y plane at the bottom of the region. These 100-second stirring motions are
111 associated with photospheric circulation, which, in this simplified model, provides a time
112 dependent deflection of magnetic field lines at the bottom boundary. These disturbances
113 propagate upwards into the MHD medium where, due to the strong imposed magnetic
114 field, the response of the fluid is limited to velocity and magnetic field fluctuations that
115 lie in transverse x-y planes, and have long wavelengths in the z-direction. The issue
116 addressed by *Dmitruk et al.* [2004] is whether a stirring force with a monochromatic time
117 dependence at the base would give rise to wave-like features in the time domain at the
118 top boundary. The height of the simulation region is assumed to be several solar radii,
119 and the transverse scales are 30,000 to 100,000 km, so this "box" is highly anisotropic and
120 extended in the vertical, mean-magnetic field aligned direction. These studies found that
121 even while strong Reduced-MHD turbulence [*Zank and Matthaeus, 1992*] is maintained in
122 the interior of the box, an enhanced spectral feature at the driving frequency persists to
123 long times at the top of the box. Put another way, this study supports the idea that a time
124 signal can, under some circumstances, persist across space, in the presence of turbulence.

125 It appears then that periodic forcing at frequency ω_0 at the coronal base can have a
126 detectable influence at the “top” of the corona. One step in establishing the feasibility
127 of persistence of p-modes in the solar wind has been thus been demonstrated. Other
128 steps in the chain also need to be examined. Suppose the solar wind with speed V_{sw} is
129 imagined as originating at a surface (perhaps this should be identified with the Alfvénic
130 critical point.) The time dependence at this surface, now originating at the top of a model
131 sub-Alfvénic corona, is converted into spatial structures with a more or less well known
132 parallel wavenumber, on the order of ω_0/V_{sw} . If the time dependence at the source surface
133 includes signals with discrete frequencies, as we have argued above may be the case, then
134 the parallel wave number structure of the fluctuations in the solar wind may demonstrate
135 a related discrete mode structure. This kind of structure would also be immersed in
136 a bath of turbulent fluctuations having other origins in the corona, perhaps associated
137 with photospheric circulation and subsequent processing due to magnetic reconnection
138 and other MHD processes. The question now arises as to whether these spatial structures
139 can survive in transit to 1 AU where they might be observed. From a basic physics
140 perspective this is a question that is complementary to the one raised by *Dmitruk et al.*
141 [2004]: *Can a wave-like spatial structure persist in time in the presence of turbulence?*
142 And, by extension, *How long does a parallel spectrum that consists of discrete modes*
143 *survive in strong turbulence?* We now address these questions.

3. Numerical approach

144 To investigate this new question we carry out a series of numerical experiments using a
145 three-dimensional (3D) compressible MHD code. The basic idea is that we set up, as an
146 initial value problem or with specific forcing terms, a magnetofluid with two spectral com-

ponents. One of them is wave-like with a fixed wavenumber parallel to the applied mean
 magnetic field. In the absence of nonlinear couplings this component would have a fixed
 Alfvén wave frequency. The other component is a field of either purely two-dimensional
 (2D) MHD fluctuations, which have zero Alfvén wave frequency (zero parallel wave num-
 ber), or quasi-2D fluctuations which have a nonzero spread in parallel wavenumber around
 the value $k_{\parallel} = 0$. Incompressible quasi-2D fluctuations are also quasi-zero-frequency.

Our simulations are based on a standard dimensionless representation of the compress-
 ible MHD system comprising the equations of continuity, momentum, and magnetic in-
 duction:

$$\frac{\partial}{\partial t} \rho = -\nabla \cdot (\rho \mathbf{u}), \quad (1)$$

$$\begin{aligned} \frac{\partial}{\partial t} \mathbf{u} = & -\mathbf{u} \cdot \nabla \mathbf{u} - \frac{1}{\rho} \nabla P + \frac{\mathbf{J} \times \mathbf{B}}{M_{a0}^2 \rho} \\ & + \frac{1}{\rho} \nu \nabla^2 \mathbf{u} + \frac{1}{\rho} \left(\zeta + \frac{1}{3} \nu \right) \nabla (\nabla \cdot \mathbf{u}), \end{aligned} \quad (2)$$

$$\frac{\partial}{\partial t} \mathbf{A} = -\mathbf{E} + \nabla F. \quad (3)$$

Here the fluid velocity is \mathbf{u} . The current \mathbf{J} is related to the magnetic field \mathbf{B} and the
 vector potential \mathbf{A} through $\mathbf{J} = \nabla \times \mathbf{B} = \nabla \times \nabla \times \mathbf{A}$. This system is closed by using an
 Ohm's law, $\mathbf{E} = -\mathbf{u} \times \mathbf{B} + \mu \mathbf{J}$, and a polytropic relation between pressure and density,
 $P = \rho^\gamma / (\gamma M_{s0}^2)$, where $\gamma = 5/3$ in this paper. The function F is chosen to preserve the
 Coulomb gauge condition, $\nabla \cdot \mathbf{A} = 0$ (see *e.g.*, Ghosh *et al.* [1993a]).

We use a pseudospectral algorithm and a periodic Cartesian geometry (see *e.g.*, Ghosh
et al. [1993a]). All dynamical fields are expanded in a truncated Fourier series such as

$$\delta \mathbf{u}(\mathbf{x}, t) = \sum_{\mathbf{k}} \delta \mathbf{u}_{\mathbf{k}}(t) \exp(i\mathbf{k} \cdot \mathbf{x}) \quad (4)$$

168 and the expansion is projected onto the pseudospectral real-space grid. Our notation
 169 is such that unless specified with a δ prefix or 0 subscript, all vectors represent the full
 170 quantity: constant plus fluctuations. Hence the magnetic field is $\mathbf{B} = \mathbf{B}_0 + \delta\mathbf{B}$, with
 171 $\mathbf{B}_0 = B_0\hat{x}$ and $B_0 = 4$. Note that $\mathbf{u}_0 = 0$ since there is no mean flow, and so $\mathbf{u} = \delta\mathbf{u}$. The
 172 two normalization coefficients are M_{s0} , a characteristic sonic Mach number, and M_{a0} , a
 173 characteristic Alfvénic Mach number. We set $M_{a0} = 1$ to run the simulations in Alfvén
 174 speed units, and $M_{s0} = 1/4$. The nominal plasma β (ratio of squared sound speed to the
 175 squared Alfvén speed) is unity.

176 The last two terms in (2) represent viscous dissipation, involving viscosity coefficients
 177 ζ and ν . We let $\zeta = 0$. Operationally, we replace the simple Laplacian dissipation
 178 coefficients with bi-Laplacian forms for the viscosity ν and the resistivity μ , which can
 179 be expressed in the transform (wavenumber k) space as $\nu_k = \nu_0[1 + (k/k_{eq})^2]$ and $\mu_k =$
 180 $\mu_0[1 + (k/k_{eq})^2]$. For the cases studied here we choose $k_{eq} = 1$, with ν_0 and μ_0 ranging
 181 between $2 \times 10^{-5} \leq \nu_0, \mu_0 \leq 5 \times 10^{-6}$ depending on the simulation’s resolution. This
 182 choice is motivated purely on computational grounds and keeps the dissipation relatively
 183 low over a broad range of the spectrum while maintaining enough damping at the high
 184 wave numbers to minimize aliasing errors. (See *e.g.*, *Borue and Orszag [1995]* or *Siregar*
 185 *et al. [1995]* for discussions on the usage of nonstandard dissipation operators.)

186 Quantities of interest in descriptions of both waves and turbulence include the fluctu-
 187 ating cross helicity $\langle \delta\mathbf{u} \cdot \delta\mathbf{B} \rangle_x$ and the fluctuating magnetic helicity $\langle \delta\mathbf{A} \cdot \delta\mathbf{B} \rangle_x$ and their
 188 associated spectra. ($\langle \dots \rangle_x$ denotes a spatial (volume) average.) Cross helicity and, in
 189 particular, its normalized value σ_c provide a measure of “Alfvénicity,” while the normal-

190 ized magnetic helicity σ_m is a measure of handedness or polarization (see *e.g.*, *Matthaeus*
 191 *and Goldstein* [1982]).

192 The simulation timescale T is the transit time of unit distance of a signal propagating at
 193 unit Alfvén speed. The length of the box is $2\pi L_0$ which defines the unit length L_0 . Hence
 194 the characteristic transit time of an ($B_0 = V_A = 1$) Alfvén wave across the box is $2\pi T$
 195 where V_A is the Alfvén speed associated with $B_0 = 1$. We will also discuss time intervals
 196 in terms of the characteristic nonlinear time: the eddy turnover time unit, $T_E = L_0/u_{\text{rms}}$,
 197 where u_{rms} is the root mean square turbulence speed. Our simulations typically run for
 198 several eddy turnover times, T_E , with a time step of $\Delta t = 0.001$.

199 We consider a three-dimensional (3D) geometry where the mean field lies in the \hat{x}
 200 direction and there are two directions, y and z , perpendicular to the mean field. The
 201 majority of our simulations are at $64 \times 64 \times 64$ resolution, which translates to modes with
 202 a maximum wave number $|k_{i,\text{max}}| = 32$ for components $i = (x, y, z)$. Here dissipation
 203 effects are negligible for scales $|\mathbf{k}| < 15$.

204 We perform two types of simulations: (1) decaying initial value cases, and (2) driven
 205 cases. We also vary Δk , the width in the k_{\parallel} direction of the spectrum of 2D fluctuations.
 206 The wave-like component, at $k_{\parallel} = 10$ has in some runs, a pure cross helicity $\sigma_c = 1$ to
 207 emulate the outward propagating nature of fluctuations that have this dominant character
 208 in the inner heliosphere. [*Bavassano and Bruno, 1995*]

4. Results

209 We first present a limiting case that demonstrates some essential features of this study.
 210 We consider the decay of an initial value state composed of a turbulence component at
 211 $k_x = 0$ and a discrete Alfvénic mode at $k_x = 10$. The turbulence component has zero

212 bandwidth in the k_{\parallel} direction ($\Delta k_x = 0$) and a flat equipartitioned spectrum of randomly
 213 excited velocity and magnetic fluctuations in the (k_y, k_z) -plane between $0 \leq |\mathbf{k}| \leq 5$. The
 214 cross helicity of each mode is zero. The fluctuating energy of the turbulence is $E_{Turb} = 1$
 215 where $E_{Turb} = \frac{1}{2} \sum_{\mathbf{k}} E(\mathbf{k}) = \frac{1}{2} \sum_{\mathbf{k}} (\delta \mathbf{u}_{\mathbf{k}} \cdot \delta \mathbf{u}_{\mathbf{k}} + \delta \mathbf{B}_{\mathbf{k}} \cdot \delta \mathbf{B}_{\mathbf{k}})$ in the range $0 \leq |\mathbf{k}| \leq 5$. The
 216 discrete mode has fluctuating energy $E_{Disc} = 0.5$ and normalized cross helicity $\sigma_c =$
 217 $2H_c/E$ equal to unity ($\sigma_c(k_x = 10) = 1$). A cartoon representation of this geometry is
 218 shown in Figure 2.

219 Within an eddy-turnover time $T_E \sim 1$ after the start of this simulation, the spectral
 220 distribution becomes more akin to the cartoon in Figure 2(b). Here, the initial turbulence
 221 at $k_x = 0$ has spread across the (k_y, k_z) plane. Similarly, wave-wave couplings between
 222 the discrete mode and turbulence form a flat sheet of fluctuations across the $k_x = 10$
 223 plane. A snapshot at $T_E = 4$ from the simulation is shown in Figure 3. Here, a grey-scale
 224 image of the magnetic power spectrum $E_b(\mathbf{k}) = (1/2) \delta \mathbf{B}_{\mathbf{k}}^* \cdot \delta \mathbf{B}_{\mathbf{k}}$ shows the power in the
 225 initial 2D turbulence has spread across the (k_y, k_z) -plane at $k_x = 0$. Similar flat sheets of
 226 fluctuation energy appear at $k_x = 10$, the location of the original discrete mode. There
 227 is also evidence of energy spreading to harmonics at $k_x = 20, 30, \dots$. We will not focus on
 228 the higher harmonics in this paper, but simply note that past studies (e.g., *GalinskyEA*
 229 [1997]) suggest these harmonics are related to the steepening of density waves associated
 230 with our initial state.

231 The full k -space geometry as depicted in Figure 3 is not what one would measure
 232 from single-point spacecraft measurements. For this, we need to return to our cartoon 3D
 233 geometry and consider what one would measure at a selected spatial location if a snapshot
 234 from our simulation box were allowed to flow past a detector at a super-Alvénic speed

\mathbf{V}_{sw} and angle Θ relative to the mean magnetic field \mathbf{B}_0 . We invoke the Taylor frozen-in
 flow assumption (see *e.g.*, *Matthaeus and Goldstein [1982]*). That is, for flows sufficiently
 faster than the oscillation period of the fluctuations, the spectrum obtained from single-
 point time measurements is determined in effect by summing all energy in wavevectors
 as projected onto the direction of flow. Here that is the \mathbf{V}_{sw} direction, designated by the
 unit vector $\hat{\mathbf{r}}$. In this way the frequency spectrum of single-point spacecraft measurements
 is interpreted as a Doppler shifted one-dimensional (1D) power spectrum along $\hat{\mathbf{r}}$. This is
 shown in Figure 4, where we draw representative directions of observation relative to the
 mean magnetic field, namely $\hat{\mathbf{r}}$ having angles of $\Theta = 10^\circ$ and 30° , lying in the (k_x, k_z) -
 plane. This represents the solar wind flow direction at angle Θ relative to the k_x -axis
 (the direction of \mathbf{B}_0). We then compute the 1D power based on the relation $E = \sum_{k_r} E_{k_r}$
 where $E(k_r) = \sum_{\{\mathbf{k}|\mathbf{k}\cdot\hat{\mathbf{r}}=k_r\}} E(\mathbf{k})$ is the 1D power spectrum along \mathbf{k}_r which depends on the
 projected wave number k_r . E_r is easily computed from our 3D simulations by binning
 (summing) the power spectrum according to the mode's projection onto the $\hat{\mathbf{r}}$ axis.

We now portray the information contained in the time snapshot of the spectrum in
 Figure 3 in terms of a 1D reduced magnetic power spectrum $E_b(k_r)$ computed for three
 choices of angle Θ . Figure 5 shows $E_b(k_r)$ for $\Theta = 1^\circ$. Here, for a flow nearly parallel
 to \mathbf{B}_0 , the 2D turbulence along the (k_y, k_z) -plane does not appear at all. The sheet of
 fluctuations on the $k_x = 10$ plane projects down to display a discrete mode at $k_r = 10$.
 Increasing the angle of flow direction to $\Theta = 10^\circ$ (Figure 4b), shows the projection of the
 2-D turbulence beginning to appear among the low- k_r modes. The sheet of fluctuations
 on the $k_x = 10$ plane projects to a k_r range spanning $7 \leq k_r \leq 10.2$. If we continue to
 increase the flow angle relative to \mathbf{B}_0 , the 2-D turbulence spans most of the k_r range while

258 the feature associated the discrete sheet at $k_x = 10$ disappears almost completely. This is
 259 shown in Figure 5(c) for $\Theta = 30^\circ$.

260 It is easy to see that if one were to average the reduced spectrum from a time interval
 261 where the flow is nearly field-aligned with another reduced spectrum from a time interval
 262 where the flow is oblique to the mean magnetic field would lead to a turbulence spectrum
 263 with embedded discrete modes. Hence, it is possible that projection effects lead to ob-
 264 served spectra having both broad band turbulence and discrete modes, even though these
 265 features could be widely separated in k -space.

266 The results shown in Figure 3 and Figure 5 are of an idealized case of zero k_{\parallel} bandwidth
 267 for both the low frequency turbulence and higher frequency discrete mode. This can be
 268 associated with cases in which the discrete mode is monochromatic and the low-frequency
 269 turbulence is sufficiently removed in frequency from the discrete mode so that $\Delta k_{\parallel} \approx 0$ is
 270 a reasonable approximation for the low frequency signal. This is a highly idealized case,
 271 and for application to the solar wind, both assumptions should be challenged. The alert
 272 reader will also note that any simulation initial state constructed with purely $k_x = 0$ and
 273 $k_x = N$ excited modes (N is any number), leads to a striated 3D spectrum composed of
 274 modes purely along $k_x = mN$ sheets where $m = 0, 1, 2, 3, \dots$ Computationally, it is easy
 275 to create entire families of discrete modes if the original state is composed of modes with
 276 zero k_{\parallel} bandwidth.

277 To characterize dynamical behavior beyond this restriction, we now introduce a non-
 278 zero k_{\parallel} bandwidth in the turbulent component at $k_x = 0$. We three consider cases where
 279 $\Delta k_{\parallel} = 1, 2, 3$, respectively. We keep the discrete mode monochromatic at $k_x = 10$, that is,
 280 without a similar bandwidth, because k_{\parallel} broadening of the discrete mode quickly develops

281 through couplings with the k_{\parallel} broadening of the turbulent component. There is no need
 282 to separately add spectral broadening to the discrete mode.

283 We run this initial state while driving the low-frequency turbulent component with
 284 random forcing such that the amplitudes of the initial turbulent modes remain constant
 285 while their phases change. This sort of forcing essentially introduces zero cross-helicity
 286 power into the simulation. Recall the discrete mode at $k_x = 10$ has $\sigma_c = 1$. If we measure
 287 the cross-helicity degradation of all modes on the $k_x = 10$ plane as a function of time, this
 288 is a direct measure of how much power is introduced at $k_x = 10$ due to nonlinear wave
 289 couplings. In this way, we use the cross helicity as a marker for nonlinear activity. Our
 290 expectation is that as the k_{\parallel} -bandwidth of the driven turbulent component increases, the
 291 rate of cross helicity decay in the $k_x = 10$ plane will increase in proportion. Hence, the
 292 preservation of the monochromatic mode at $k_x = 10$ will be directly correlated with the
 293 relative k_{\parallel} bandwidth of the turbulent component.

294 We find this to be precisely the case as shown in Figure 6(a). Here, we compare the time-
 295 evolution of $\sigma_c(k_x = 10)$, the normalized cross-helicity in the $k_x = 10$ plane for cases in
 296 which $\Delta k_{\parallel} = 0, 1, 2, 3$. Based on the energy of the driven turbulence, our normalized time
 297 units are roughly equivalent to an eddy-turnover time. Comparing the simulations at time
 298 $T = 2$, we see our original idealized case, $\Delta k_{\parallel} = 0$, decays the least with $\sigma_c(k_x = 10) \approx 0.9$.
 299 For $\Delta k_{\parallel} = 1$ we find $\sigma_c(k_x = 10) \approx 0.7$, for $\Delta k_{\parallel} = 2$ we find $\sigma_c(k_x = 10) \approx 0.5$, and
 300 finally for $\Delta k_{\parallel} = 3$ we find $\sigma_c(k_x = 10) \approx 0.3$. That is, the wider the frequency dispersion
 301 in the low frequency turbulence, the more rapid is the degradation of the monochromatic
 302 discrete mode.

303 The presence of a mean magnetic field strongly influences this result. As shown in
304 Figure 6(b), if we run the same simulations with $B_0 = 0$, all runs with $\Delta k_{\parallel} \neq 0$ decay
305 at roughly the same rate. The $\Delta k_{\parallel} = 0$ decays at the same rate as the $B_0 \neq 0$ case,
306 confirming our earlier assertion that the zero bandwidth case is idealized and not directly
307 applicable to physical reality.

308 We have rerun all these simulations at the higher resolution of $128 \times 128 \times 128$, and
309 proportionately lower dissipation, and find that our results do not change qualitatively.

310 Finally, we return to the frequency-domain problem studied by *Dmitruk et al.* [2004]
311 and repose the question in the wavenumber-domain, and in our present periodic fully
312 3D domain. Previously, using a Reduced-MHD formalism, *Dmitruk et al.* [2004] found
313 that single-frequency stirring at the base of a 3D non-periodic box simulation leads to
314 monochromatic point-spectral feature in the frequency spectrum measured at the top of
315 the box. Such frequency spectra are preserved even while turbulence is maintained inside
316 the box. In a similar manner, we can ask what happens to the wavenumber spectrum of
317 a driven monochromatic mode in the presence of driven low- k turbulence? Interestingly,
318 as shown in Figure 7, the monochromatic nature can be preserved in the k -space domain.
319 Here, we run a 3D simulation with a randomly driven ball of background turbulence at
320 $|\mathbf{k}| \leq 5$ and a similarly driven monochromatic mode at $(k_x, k_y, k_z) = (9, 5, 0)$ in the pres-
321 ence of a mean magnetic field in the k_x -direction. Figure 7 shows a surface plot of the
322 magnetic power in the $k_z = 0$ plane at $T = 6$, which is several eddy-turnover times into the
323 run. The turbulence cascade is well-developed. Nevertheless, the driven monochromatic
324 mode is easily discernable from the surrounding turbulence. This contradicts any assump-
325 tion that a driven mode smoothly couples with its adjacent modes so as to destroy its

326 discrete nature. The associated grey-scale contour plot of the magnetic power is shown in
327 Figure 8. Here too, the discrete mode is easily discernable. Anisotropy is apparent in the
328 magnetic spectrum [*Shebalin et al.*, 1983] in the sense that spectral transfer is suppressed
329 in the wavenumber direction parallel to the mean magnetic field.

330 The relation of the Figure 7 result to the *Dmitruk et al.* [2004] study is not direct.
331 The Dmitruk study considers a stationary frame of reference representing the solar sur-
332 face at the bottom and a surface several solar radii outward at the top. On the other
333 hand, our periodic-box studies represent a box co-moving with the outwardly flowing solar
334 wind. Nevertheless the present result, with implications for persistence of wave number
335 structures, is clearly complementary to the earlier results on persistence of features in the
336 frequency domain.

5. Discussion and Conclusions

337 Motivated by reports suggesting the presence of discrete, reproducible modes in the so-
338 lar wind that are in the frequency ranges corresponding to solar internal pressure (p) and
339 gravity (g) modes, a controversy persists in the magnetohydrodynamic (MHD) turbulence
340 community whether discrete modes (independent of their source) can persist in the pres-
341 ence of a turbulent cascade. We have performed a series of direct numerical simulations
342 of a compressible 3D MHD system to examine whether such coexistence is feasible, and if
343 so, under what circumstances. We find two scenarios: First, in the presence of a DC mag-
344 netic field, turbulent cascades are known to be suppressed in the field-parallel direction.
345 In this case, a discrete mode can persist for several nonlinear times without interacting
346 strongly with the turbulence if its wavevector component parallel to the DC magnetic field
347 is significantly larger than the k-space bandwidth of the turbulent cascade variation in

348 the field-parallel direction. Second, for sufficiently weak forcing a driven mode can persist
349 as a discrete mode despite being deeply embedded inside a driven turbulence cascade. In
350 this case, the mode does not display spectral broadening, nor does the spectrum of the
351 adjacent turbulence depart from a Kolmogoroff-like cascade. We also examined projection
352 effects of the full k-space onto a direction of observation, producing a 1D reduced spec-
353 trum, as typical of single-spacecraft observations. The results suggest that the discrete
354 mode is more likely to be observed when the angle between solar-wind flow direction and
355 the DC magnetic-field direction is small. This study complements driven reduced MHD
356 simulations of a model of the solar corona *Dmitruk et al.* [2004] that support similar
357 conclusions based on time-domain (frequency) analysis.

358 A natural question is how do these results relate to the seemingly contradictory results of
359 *Roberts et al.* [1996]? Their argument is based on 1D simulations. In the 1D case, Alfvénic
360 and other incompressive fluctuations couple to one another only via the acoustic channel in
361 a fashion akin to parametric instabilities (see *e.g.*, *Ghosh et al.* [1993b]). No incompressive
362 three-wave couplings characteristic of 2D and 3D geometries are permissible. Hence,
363 the 1D model dramatically enhances the influence of compressibility while the full 3D
364 geometry permits sufficient energy transfers through incompressive wave-wave couplings
365 so that the influence of compressibility is significantly less. Our simulations without a
366 mean magnetic field, as shown in Figure 6(b), fall closer to the 1D simulations of *Roberts*
367 *et al.* [1996] because even though incompressive wave-wave couplings are competing with
368 compressive wave-wave couplings, no direction is preferentially selected to distinguish one
369 type of mode-mode coupling over another. And similar to the Roberts result, all our

370 simulations with $B_0 = 0$ show rapid destruction of the discrete mode when the perturbing
371 turbulence has a finite bandwidth in parallel wavenumber.

372 To summarize, the persistence of a discrete mode with turbulence appears to rest on two
373 conditions: First, a background (mean) magnetic field must be present; and second, there
374 must be sufficient wavenumber separation between the k_{\parallel} bandwidth of the background
375 turbulence and the k_{\parallel} wavenumber of the discrete mode for nonlinear couplings to proceed
376 more efficiently in the plane orthogonal to the mean magnetic field than along the direction
377 of the mean magnetic field. In the present study we have focused on the wavevector
378 structure of the turbulence and the discrete modes, in contrast to the *Dmitruk et al.* [2004]
379 study that focused on Eulerian frequency spectra. However we note that wide separation
380 in k_{\parallel} along with a finite B_0 necessarily implies wide separation in wave frequency. The
381 dual constraints of frequency and wave number matching [*Shebalin et al.*, 1983], restrict
382 parallel spectral transfer. Under the right conditions this can lead also to survival of
383 discrete modes.

384 Finally we remark on the possible connection between the crucial issue of k_{\parallel} bandwidths
385 and random motions in the lower corona and photosphere. The full complexity of this
386 problem is far beyond the scope of the present paper. However a useful remark can be
387 made based on the quasi-static model [*Giacalone et al.*, 2006] in which the solar wind
388 emerges from a surface at which the speed V_{sw} is determined, beginning suddenly from
389 a plane containing the modeled photospheric motions. Expansion is ignored in a first
390 approximation. In this simple model it is readily demonstrated that the k_{\parallel} structure
391 emerges from the time dependence of the photospheric motions. The k_{\parallel} wavenumber of a
392 discrete mode in the solar wind would be determined by a coherent oscillation at frequency

393 ω_0 in the photosphere, giving a discrete wavenumber $k_{\parallel}^0 = \omega_0/V_{sw}$. We associate this, for
 394 example, with a p-mode. In addition we suppose there is a strong nearly steady k_{\perp}
 395 spectrum of photospheric motions that give rise to activity near $k_{\parallel} = 0$ in the solar
 396 wind. However slow variations and temporal decorrelation of these nearly steady motions
 397 impose a spectral distribution with bandwidth of $\Delta\omega$ around zero frequency. Thus the
 398 random photospheric motions give rise to a solar wind spectral component with $\Delta k_{\parallel} =$
 399 $\delta\omega/V_{sw}$ near $k_{\parallel} = 0$. In the simplest approximation, the correlation time is related
 400 to the bandwidth by $\tau_c = 1/(\Delta\omega)$. The condition for persistence of the discrete mode
 401 is $k_{\parallel}^0 \gg \Delta k_{\parallel}$, or, equivalently $\omega_0\tau_c \gg 1$. Taking $\omega_0 \sim 1/300$ seconds (a typical
 402 5-minute ‘‘p-mode’’ oscillation) gives the condition on the correlation time $\tau_c \gg 300$
 403 seconds. Therefore, if photospheric motions decorrelate in 1000 seconds it is unlikely to
 404 see persistence of discrete modes to 1 AU, but if they persist for $\tau_c > 10,000$ seconds,
 405 conditions for persistence might be favorable. We defer a more detailed examination of
 406 this possibility to future studies.

407 **Acknowledgments.**

408 This work was supported by NASA grants NNG06GD47G, NNX07AB11G,
 409 NNX07AV49G, NNG06GE65G, subcontract LANL 11748-001-05, and NSF grants ATM-
 410 0539995 and ATM-0752135. DJT’s research is supported by the Canada Research Chairs
 411 program and NSERC.

References

412 Bavassano, R., and R. Bruno (1995), Density fluctuations and turbulent Mach numbers
 413 in the inner solar wind, *J. Geophys. Res.*, **100**, 9475.

- 414 Borue, V., and S. A. Orszag (1995), Self-similar decay of three-dimensional homogeneous
415 turbulence with hyperviscosity, *Phys. Rev. E*, **51**, R856.
- 416 Denison, D. G. T., and A. T. Walden (1999), The search for gravity-mode oscillations:
417 an analysis using Ulysses magnetic field data, *Ap J*, *514*, 972–978.
- 418 Dmitruk, P., W. H. Matthaeus, and L. J. Lanzerotti (2004), Discrete modes and turbu-
419 lence in a wave-driven strongly magnetized plasma, *Geophys. Res. Lett.*, **31**, L21805,
420 doi:10.1029/2004GL021119.
- 421 Galinsky, V. L.; Shevchenko, V. I.; Ride, S. K.; Baine, M., Excitation of nonlinear Alfvén
422 waves by an ion beam in a plasma 1. Right-hand polarized waves, *J. Geophys. Res.*,
423 **102**, 22365–22376.
- 424 Ghosh, S., M. Hossain, and W. H. Matthaeus (1993a), The application of spectral methods
425 in simulating compressible fluid and magnetofluid turbulence, *Comp. Phys. Comm.*, **74**,
426 18.
- 427 Ghosh, S., A. F. Viñas, and M. L. Goldstein (1993b), Parametric instabilities of a large-
428 amplitude circularly polarized Alfvén wave: Linear growth in two-dimensional geome-
429 tries, *J. Geophys. Res.*, **98**, 15 561.
- 430 Giacalone, J., J. R. Jokipii, and W. H. Matthaeus (2006), Structure of the turbulent
431 interplanetary magnetic field, *Astrophys. J.*, **641**, L61–L64.
- 432 Hoogeveen, G. W., and P. Riley (1998), The search for solar gravity-mode oscillations in
433 the solar wind using *ulysses* plasma data, *Solar Phys.*, **179**, 167–177.
- 434 Lanzerotti, L. J., R. E. Gold, K. A. Anderson, T. P. Armstrong, R. P. Lin, S. M. Krimigis,
435 M. Pick, E. C. Roelof, E. T. Sarris, G. M. Simnett, and W. E. Frain (1992), Heliosphere
436 instrument for spectra, composition, and anisotropy at low energies, *Astronomy and*

- 437 *Astrophysics Suppl. Ser.*, **92**, 349–363.
- 438 Matthaeus, W. H., and M. L. Goldstein (1982), Measurement of the rugged invariants of
439 magnetohydrodynamic turbulence in the solar wind, *J Geophys. Res.*, **87**, 6011–6028.
- 440 McComas, D. J., S. J. Bame, P. Barker, W. C. Feldman, J. L. Phillips, P. Riley, and J. W.
441 Griffee (1998), Solar wind electron proton alpha monitor (SWEPAM) for the Advanced
442 Composition Explorer, *Space Science Reviews*, **86**, 563–612.
- 443 Provost, J., G. Berthomieu, and P. Morel (2000), Low-frequency p - and g -mode solar
444 oscillations, *A & A*, **353**, 775–785.
- 445 Roberts, D. A., K. W. Ogilvie, and M. L. Goldstein (1996), The nature of the solar wind,
446 *Nature*, **381**, 31–32.
- 447 Shebalin, J. V., W. H. Matthaeus, and D. Montgomery (1983), Anisotropy in MHD
448 turbulence due to a mean magnetic field, *J. Plasma Phys.*, **29**, 525–547.
- 449 Siregar, E., S. Ghosh, and M. L. Goldstein (1995), Nonlinear entropy production operators
450 for magnetohydrodynamic plasmas, *Phys. Plasmas*, **2**, 1480.
- 451 Thomson, D. J. (1982), Spectrum estimation and harmonic analysis, *Proc. IEEE*, **70**,
452 1055–1096.
- 453 Thomson, D. J., C. G. MacLennan, and L. J. Lanzerotti (1995), Propagation of solar
454 oscillations through the interplanetary medium, *Nature*, **376**, 139.
- 455 Thomson, D. J., L. J. Lanzerotti, and C. G. MacLennan (2001), The interplanetary mag-
456 netic field: Statistical properties and discrete modes, *J. Geophys. Res.*, **106**, 15.
- 457 Thomson, D. J., L. J. Lanzerotti, F. L. Vernon, III, M. R. Lessard, and L. T. P. Smith
458 (2007), Solar modal structure of the engineering environment, *Proc. IEEE*, **95**, 1085–
459 1132.

- 460 Tu, C.-Y., and E. Marsch (1995), MHD structures, waves and turbulence in the solar
461 wind, *Space Sci. Rev.*, **73**, 1–210.
- 462 Zank, G. P., and W. H. Matthaeus (1992), The equations of reduced magnetohydrody-
463 namics, *J. Plasma Phys.*, **48**, 85–100.

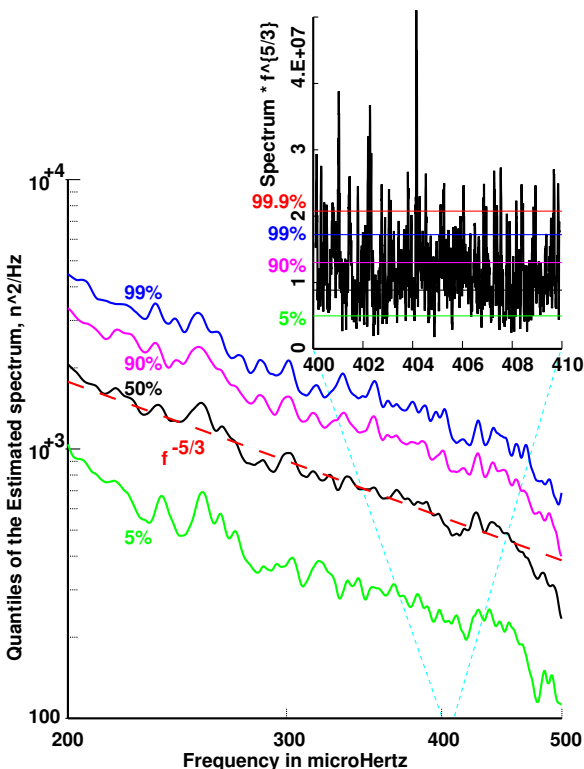
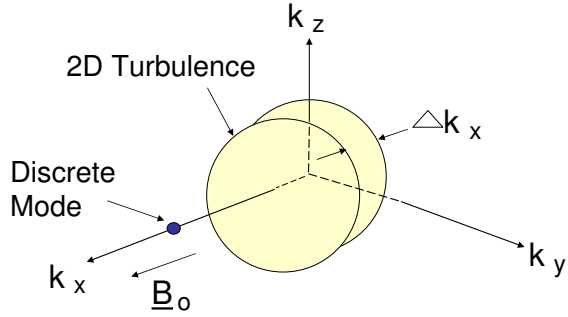
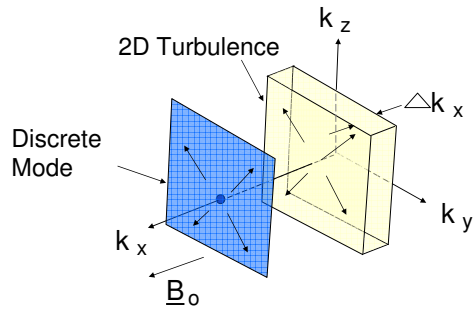


Figure 1. Quantiles of the power spectrum of proton density fluctuations on ACE between Feb. 5, 1998 and Nov. 23, 2005 in the range of 200–500 μHz . The lines, from bottom to top show the 5%, 50%, 90%, and 99% points of the spectra in $\sim 4 \mu\text{Hz}$ intervals. The step slope starting at $\sim 450 \mu\text{Hz}$ is the start of the rolloff of the $> 70 \text{ dB}$ antialias filter and the dashed red line superimposed on the 50% curve shows a $f^{-5/3}$ slope. The insert shows the same spectrum multiplied by $f^{+5/3}$ (with f in μHz) on a linear scale over the frequency range 400 to 410 μHz . Note the large peak at 404.157 μHz and the two approximately symmetric sidebands.



a) Time = 0



b) Time > 0

Figure 2. K-Space geometry of the simulation model. (a) Initial k -space geometry showing location of discrete mode at $k = (10, 0, 0)$ and initial background turbulence centered on $k_x = 0$ with bandwidth $k_{||} = \delta k$. (b) Diagram of k -space evolution as the discrete mode spreads across the $k_x = 10$ plane and the background turbulence spreads across the $k_x = 0$ plane while retaining the original $k_{||} = \delta k$ bandwidth.

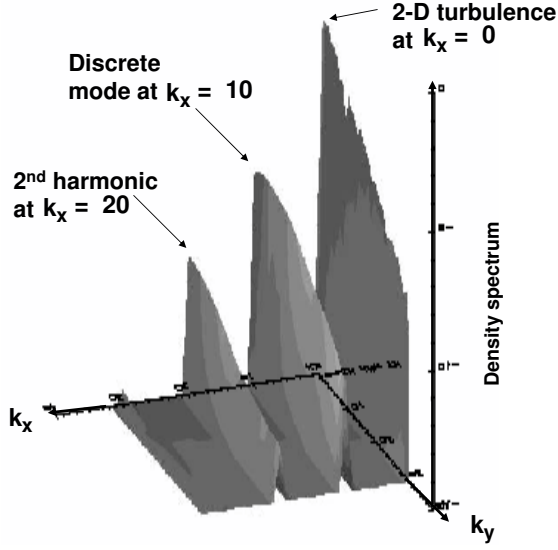


Figure 3. Magnetic power spectrum at time $T_E = 4$ from the 3D MHD simulation. The background turbulence spreads across the $k_x = 0$, the discrete mode spreads across the $k_x = 10$ plane. Nonlinear couplings between the background turbulence and the discrete mode create additional harmonics at $k_x = 20$ and $k_x = 30$.

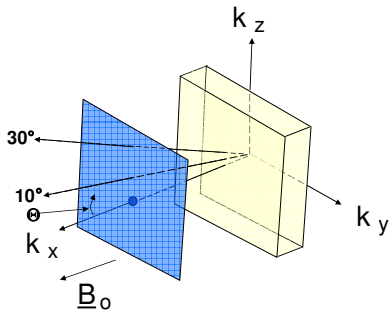


Figure 4. K-Space geometry for obtaining 1D reduced spectra from 3D simulation. Projecting 3D spectral power onto a direction Θ from the k_x -axis creates 1D reduced spectra along that direction.

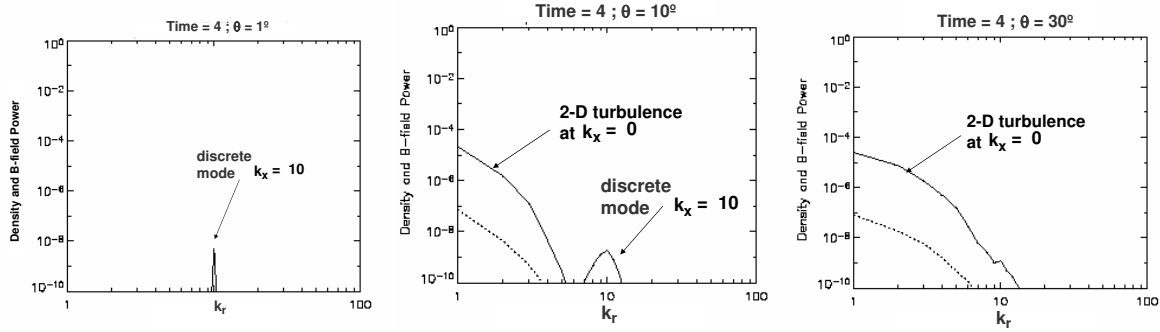


Figure 5. Reduced power spectra $E_{b,r}$ at time $T=4$ as a function of angle to mean magnetic field, computed from the spectral data in Figure 3. (a) $\theta_r = 1^\circ$, (b) $\theta_r = 10^\circ$, (c) $\theta_r = 30^\circ$. The discrete wave mode appears at small angles while the background low frequency turbulence dominates large angles.

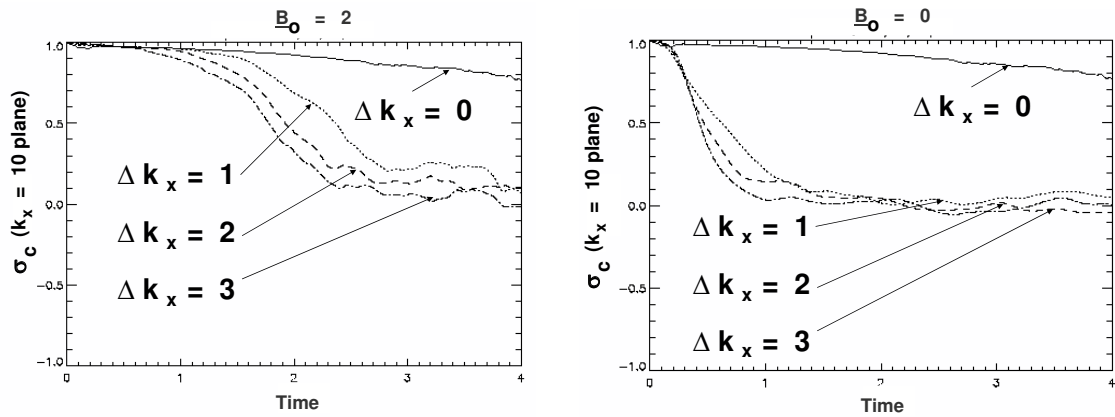


Figure 6. Time evolution of normalized cross helicity as a function of background turbulence bandwidth δk in the presence and absence of a mean magnetic field. Time evolutions of the normalized cross helicity computed on the $k_x = 10$ plane for background turbulence bandwidths $\delta k = 0$ (solid line), $\delta k = 1$ (dotted line), $\delta k = 2$ (dashed line), $\delta k = 3$ (dot-dashed line) in (a) the presence of a mean magnetic field, and (b) the absence of a mean magnetic field.

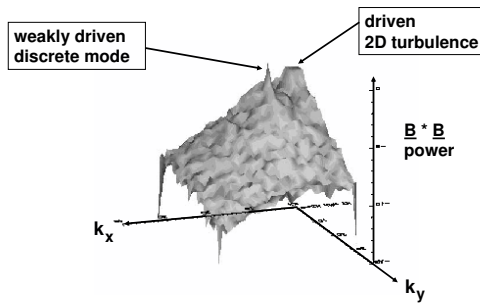


Figure 7. Magnetic power surface plot from a driven 3D MHD simulation. Power in the k_x - k_y plane at $k_z = 0$ shows the driven discrete mode at $(k_x, k_y, k_z) = (9, 5, 0)$ clearly visible above the driven background turbulence.

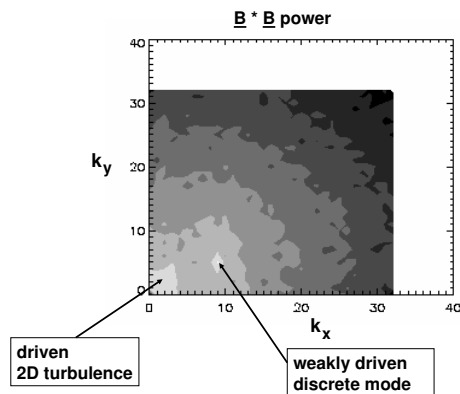


Figure 8. Magnetic power grey-scale contour of Figure 7. Again the driven discrete mode is clearly visible above the underlying turbulence. The underlying turbulence displays spectral anisotropy as expected whenever a mean magnetic field is present.